2019

Potential flow models for the heliosphere and their comparision to 3D MHD-neutral simulation

Shanti Kumari Thagunna

POTENTIAL FLOW MODELS FOR THE HELIOSPHERE AND THEIR COMPARISION TO 3D MHD-NEUTRAL SIMULATION

by

SHANTI KUMARI THAGUNNA

A THESIS

Submitted in partial fulfillment of the requirements
for the degree of Masters of Science
in
The Department of Department of Space Science
to
The School of Graduate Studies
of
The University of Alabama in Huntsville

HUNTSVILLE, ALABAMA

2019

In presenting this thesis in partial fulfillment of the requirements for a The School of Graduate Studies degree from The University of Alabama in Huntsville, I agree that the Library of this University shall make it freely available for inspection. I further agree that permission for extensive copying for scholarly purposes may be granted by my advisor or, in his/her absence, by the Chair of the Department or the Dean of the School of Graduate Studies. It is also understood that due recognition shall be given to me and to The University of Alabama in Huntsville in any scholarly use which may be made of any material in this thesis.

Shanti

Shanti Kumari Thagunna

3/26/2019

(date)

THESIS APPROVAL FORM

Submitted by Shanti Kumari Thagunna in partial fulfillment of the requirements for the degree of Masters of Science in Space Science and accepted on behalf of the Faculty of the School of Graduate Studies by the thesis committee.

We, the undersigned members of the Graduate Faculty of The University of Alabama in Huntsville, certify that we have advised and/or supervised the candidate of the work described in this thesis. We further certify that we have reviewed the thesis manuscript and approve it in partial fulfillment of the requirements for the degree of Masters of Science in Space Science.

Dr. Jacob Herrikhusien	3-26-19 (Date)	Committee Chair
Dr. Vladimir Florinski	3/26/2019 (Date)	
Dr. Jakobus le Roux	3/26/2019 (Date)	
Dr. Gary Zank	3/26/19 (Date)	Department Chair
Dr. Sundar Christopher	3/26/19 (Date)	College Dean
Dr. David Berkowitz	4/4/19 (Date)	Graduate Dean

ABSTRACT

School of Graduate Studies
The University of Alabama in Huntsville

Degree Masters of Space Science College/Dept. Science/Space Science

Name of Candidate Shanti Kumari Thagunna

Title Potential Flow Models For The Heliosphere And Their Comparison To 3D MHD-Neutral Simulation

Various models have been proposed for the SW-LISM plasma interaction to study the shape of the heliosphere. According to the Parker model (1961), when SW interacts with the interstellar plasma with a very weak magnetic field a "comet-like" cavity is formed, called heliosphere. With the help of simplified assumptions, we solve the Parker model for the heliosphere in addition with charge-exchange term and compare it with 3D MHD-neutral simulation results for the heliosphere. We develop a chi-square analysis to quantify the relative difference between 2D potential flow and 3D simulation model heliospheric models, and use this to optimize the flow model parameters to derive a simple model for the flow of SW in the inner heliosheath.

Abstract Approval: Committee Chair 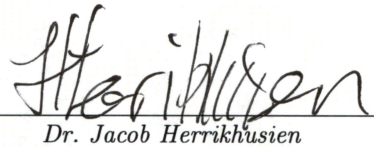
Dr. Jacob Herrikhusien

Department Chair 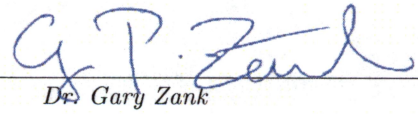
Dr. Gary Zank

Graduate Dean 
Dr. David Berkowitz

ACKNOWLEDGMENTS

I would first like to thank my supervisor Dr. Jacob Heerikhuisen for his continuous support and encouragement. Without him, it wouldn't be possible for me to finish this thesis on time. I also want to thank Dr. Vladimir Florinski and Dr. Jakobus Le Roux for being in my committee member.

I would also like to thank Mr. Bishwas lal Shrestha and Dr. Laxman Adhikari for their kind suggestions, support, and motivation.

TABLE OF CONTENTS

LIST OF FIGURES

LIST OF SYMBOLS

SYMBOL	DEFINITION
$\mathbf{u}$	Solar wind flow velocity
$\mathbf{E}$	Stellar electric field
$\mathbf{B}$	Stellar magnetic field
$\mathbf{P}$	Total pressure
Φ	flow potential
Φ_1	potential due to radial flow
Φ_2	potential due to presence of charge-exchange
ν_{ex}	charge-exchange rate
γ	adiabatic index
σ	charge-exchange cross section

To My Family

Never Lose a Holy Curiosity

—Albert Einstein

CHAPTER 1

INTRODUCTION

1.1 Solar Wind

The temperature of the outer layer of the Sun, called the corona, is up to 2 million degrees Kelvin. The Sun's gravity is unable to contain the coronal plasma because of this high temperature, and fast-moving particles escape away radially in the form of a stream of ionized plasma. This stream of ionized plasma is called solar wind (SW). The properties of the SW changes with time as the sun's activity changes throughout the 11-year solar cycle. The velocity of the SW is related to a solar activity which itself is a function of heliographic latitude.

Broadly speaking, the SW can be divided into two states: slow SW and fast SW. At solar minimum (when there are very few sunspots), slow SW originates at latitudes up to 30° - 35° in the equatorial band and has speed of $\sim$ 450 km/s and expands towards the poles as the solar cycle approached maximum (period of maximum solar activity when there are many sunspots). Fast SW originates from the polar region and has the velocity $\sim$ 800 km/s (McComas et al., 2003, 2008).

We have known about the SW since the 1950's (Gringauz et al., 1960). Several missions led the search for the reason behind it's evolution. The Ulysses mission

(November 1990 - June 2009) measured various properties of the SW for the first time by orbiting out of the solar ecliptic plane (McComas et al., 2003, 2008). STEREO - A and STEREO - B, launched in 2006 studied the Sun's edge to see how the SW evolves (Kaiser et al., 2008).

1.2 Local Interstellar Medium

The Interstellar Medium (ISM) is the matter that exists between the stars of our Galaxy. The Local Interstellar Medium (LISM) is the part of ISM around the heliosphere which extends on the order of 1000 AU from the Sun. The study of the LISM plays a significant role in understanding physical processes such as structure and evolution, gas dynamics, pressure balance and effects of cosmic radiation field on the heliosphere.

We cannot measure the undisturbed LISM properties directly. Instead we must utilize indirect measures such as neutral atoms (e.g. Ulysses (Witte, 2004), IBEX (McComas et al., 2015)). These measurements suggest that the plasma velocity and temperature are $V_\infty = 25.4$ km/s, $T_\infty = 7500$ K. Models can then be used to estimate the LISM density and magnetic field (e.g. Heerikhuisen et al. (2014); Zirnstein et al. (2016)).

1.3 Heliosphere

The word "heliosphere" in the scientific literature was first proposed by Alexander J. Dessler (Dessler, 1967). When supersonic SW plasma moves radially outward, it interacts with the LISM plasma and turns away from the incoming LISM flow

creating comet shaped structure called the heliosphere. Therefore, the heliosphere is the region of space extending about 120 AU in the direction of the motion of the Sun and may be tens of thousands of AU in the heliotail direction (Zank, 2015). The interaction between the SW and the interstellar plasma has a significant role in determining the outer structure of the heliosphere. This interaction creates a "nose" in the direction of the flow of the SW and an elongated "tail" in the opposite direction.

1.4 Structure of the Heliosphere

When the SW interacts with the LISM, the heliosphere is formed. So, the structure of the heliosphere is dependent on the LISM, the SW, and the overall motion of the Sun. The supersonic SW coming from the Sun becomes subsonic at the heliospheric termination shock (HTS) where it begins to interact with the interstellar medium plasma. The boundary that separates the SW and LISM plasma is called the heliopause (HP). The region in between the HTS and HP is the called the inner heliosheath (IHS) and the region just beyond the heliopause is called the outer heliosheath (OHS).

1.4.1 Termination Shock

The termination shock is the boundary where the supersonic SW plasma becomes subsonic and heated. Since the solar wind is slower downstream of the termination shock, the plasma becomes hotter. Voyager 1 and Voyager 2 crossed the termination shock in 2004 (Stone et al., 2005) and in 2007 (Decker et al., 2008; Stone, 2008) at 94 AU and 84 AU from Sun respectively. This shows the asymmetry in the

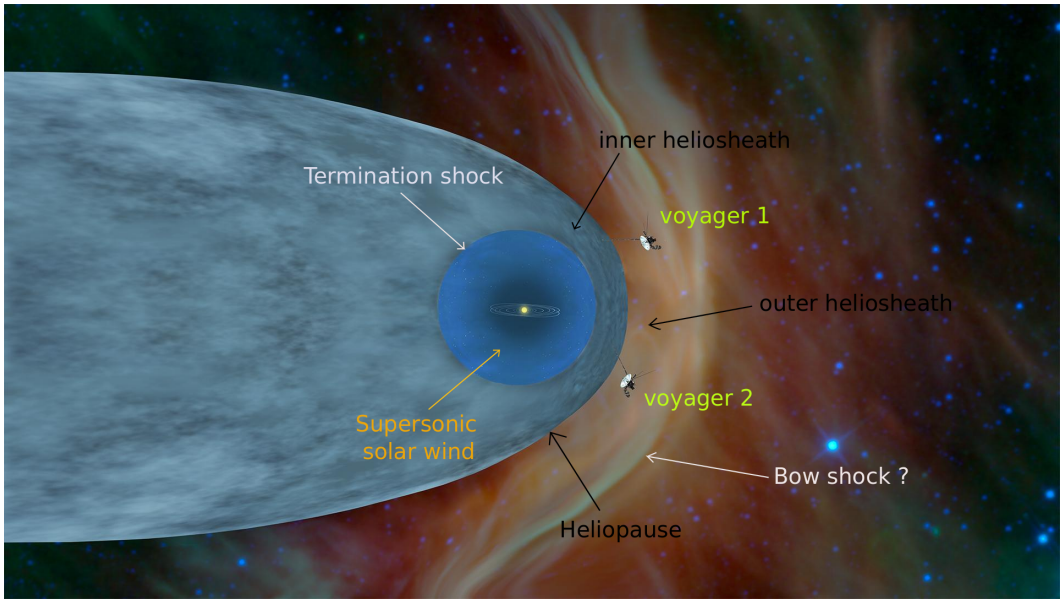

Figure 1.1: Classical comet-shaped structure of the heliosphere (Source: NASA/JPL)

termination shock which is likely due to time-dependent effects (Zank, 2015). Various other ideas have been proposed to explain the asymmetry, including turbulence and fluctuations in the shock position (Florinski, 2009).

1.4.2 Inner Heliosheath

The region in between the HTS and HP is called the inner heliosheath. The IHS has a relatively low flow speed $\sim$ 100 kms^{-1} directed away from radial direction, high temperature and densities and larger magnetic fields (Zank, 2015). According to Voyager 2 measurements of proton temperature downstream of the TS $\sim$150,000 K (Richardson, 2008; Richardson et al., 2008) which is an order of magnitude less than that predicted by global heliospheric model. The remainder of the thermal energy likely goes to heating pick up ions (PUIs) at the TS (Zank et al., 1996).

The PUIs are created by charge-exchange of interstellar neutrals with the SW protons. The main sources of PUIs in the IHS are interstellar neutral atoms that drift across the HP and charge exchange with hot SW plasma, and PUIs convected across the HTS into the IHS (Zank et al., 2014).

PUIs that convect across the HTS can be subdivided into those that are directly "transmitted", and those that are energized by "reflection" at the cross-shock potential before being convected across (Zank et al., 1996; Lee et al., 1996; Zank et al., 2010). The transmitted PUIs temperature downstream of the HTS is estimated to be ~ 0.84 keV and reflected protons have a temperature estimated to be ~ 6.6 keV (Zank et al., 2010). A third population of PUIs in the IHS are ones that are "injected" locally through charge-exchange.

Proton and electron times are greater than characteristic flow time, these types of collisions cannot equilibrate the three populations of PUIs with "core" SW in the IHS on the length scale of at least 10,000 AU (Zank et al., 2014) . Therefore, a multifluid model is needed to describe coupled SW -PUI plasma (Zank, 2015).

1.4.3 Heliopause

The Heliopause (HP) is a tangential discontinuity (across which there is no particle transport) between the SW and the LISM. At the heliopause the normal components of the magnetic field and plasma flow velocity are zero on both sides, and also the sum of the thermal pressure and magnetic pressure is equal on both sides. Voyager 1 crossed the heliopause in 2012 at 121 AU (Webber and McDonald, 2013; Stone et al., 2013). Voyager 1 determined the location of heliopause by observing an

increase of galactic cosmic ray particles and decrease in SW particles after crossing the boundary. Voyager 2 crossed the HP at 119 AU in late 2018 (AGU, 2018).

1.4.4 Outer Heliosheath

The outer heliosheath is the region of space outside the HP that is modified by the presence of the heliosphere. In models, it generally extends a few hundred AU beyond the HP, and may be bounded by a bow shock ahead of the heliosphere if the conditions permit a shock (McComas et al., 2012; Zank et al., 2012). The OHS contains PUIs that are injected when ENA's escaping the heliosphere charge exchange (Zirnstein et al., 2014). Such PUIs can be linked to the ribbon observed by IBEX spacecraft (Heerikhuisen et al., 2014). Moreover, the Interstellar Magnetic Field (ISMF) lines are compressed and draped around the heliopause leading to a deformation of the heliopause surface. This process has important significance to the study of the SW-LISM interaction (Zirnstein and McComas, 2015; Isenberg et al., 2015).

1.4.5 Models For The SW-LISM Interaction

When SW plasma from Sun moves radially outward, it interacts with the interstellar plasma via charge-exchange. Therefore, charge-exchange has a very important role in determining the shape of the heliosphere. Various models with different assumptions were proposed to deal with the SW-LISM interaction in simplified form. Some of the approaches are discussed in this section.

1.4.5.1 Parker's Model

In 1961, Parker proposed the following three models for the SW-LISM plasma interaction:

I) Static interstellar medium without interstellar magnetic field: This model is very simple as the interstellar plasma is without magnetic field and static. So, the SW flow is assumed to be spherical with little physical interest.

II) Steady subsonic interstellar wind without interstellar magnetic field (weak magnetic field, $|\mathbf{B}|= 0$): In this model SW-LISM plasma is treated hydrodynamically because of a very weak magnetic field. The flow velocity of plasma is $\mathbf{u} = -\rho^{\frac{1}{2}}\nabla\phi$ and the scalar potential is given by

$$\phi = -\rho_i v r \cos\theta + \rho_2 u_2 \frac{R^2}{r}, \tag{1.1}$$

Where ρ_i is the density in the interstellar medium, v is the interstellar velocity, R is the distance of TS from Sun, ρ_2 is the density in the downstream of termination shock, u_2 is the SW speed in the downstream of termination shock, θ is the polar angle and r is radial distance.

This model gives the comet-shaped structure of the heliosphere as shown in Figure (1.2).

III) Large-scale interstellar field in the absence of significant interstellar gas pressure and interstellar wind (strong magnetic field, $|\mathbf{B}| \neq 0$, and $\mathbf{V}_{LISM} = 0$):

In this model large-scale interstellar magnetic field is taken into consideration. According to this model the shape of the heliosphere and the direction of flow depends

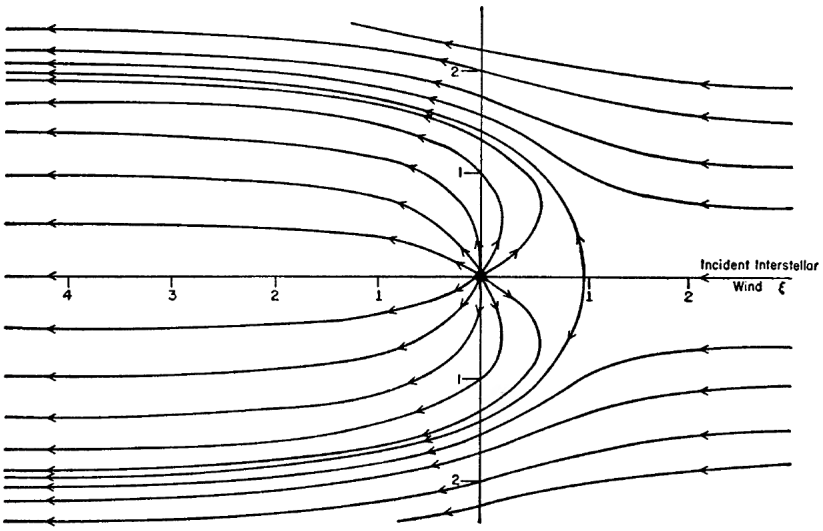

Figure 1.2: The streamlines of the subsonic, nearly incompressible, hydrodynamic flow of a stellar wind beyond the shock transition (r = R) in the presence of a subsonic interstellar wind carrying no significant magnetic field.(Parker, 1961)

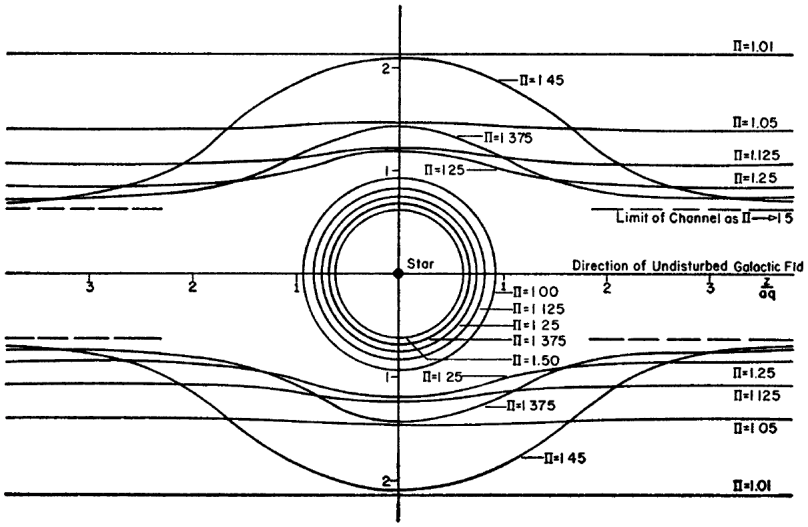

Figure 1.3: The shock transition r = R, shown by the concentric circles, and the outer boundary stellar-wind region in the presence of a large-scale interstellar magnetic field, for various values stagnation pressure at infinity (Parker, 1961)

on pressure at infinity. The shape of the heliosphere changes from a circular cylinder of infinite radius, to bulbous shape of finite radius, to a sphere of infinite radius with one finite cylindrical lobe from each pole as shown in Figure (1.3).

1.4.5.2 Global simulations of the heliosphere

To deal with the problem of including the charge-exchange of the plasma with neutral hydrogen we need to consider the multiple populations of neutral atoms and potentially also the different populations of the plasma ions. To solve such a problem, the Parker model (hydrodynamic treatment) is not sufficient. Instead, global simulations based on magnetohydrodynamics are used to study the structure of the global heliosphere. The complexity of this simulation is that the heliosphere loses its symmetry to become fully three dimensional.

Modern simulations of the SW-LISM plasma interaction are based on a 3D-MHD implementation, coupled to either fluid (Pauls and Zank, 1997; Ratkiewicz et al., 2008; Washimi et al., 2007) or particle (Heerikhuisen et al., 2008; Izmodenov and Alexashov, 2005) neutrals.

Double Tail

According to the magnetohydrodynamic(MHD) simulation by Opher (Opher, 2015), beyond the TS magnetic field is twisted and strong enough to confine the SW plasma. The confined SW plasma drives jets to the north and south lobes and are deflected into the tail region by the motion of the Sun. The force due to interstellar plasma is not strong enough to force the lobes into single comet-like shape and gives

"Croissant-like" shape as shown in Figure (1.4). No other 3D simulations reproduce this result.

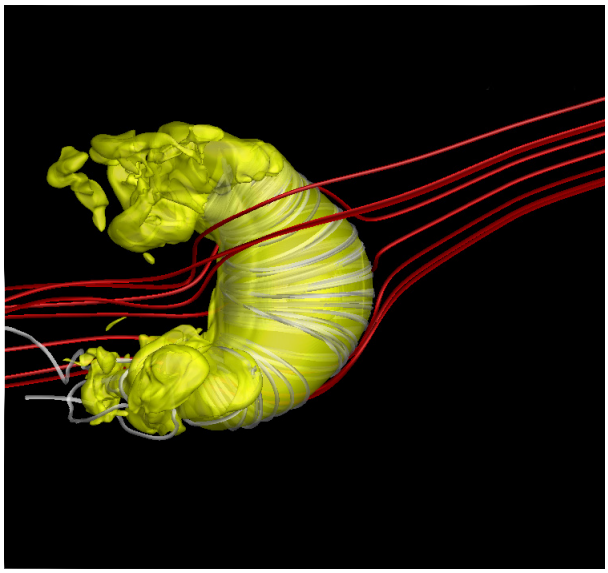

Figure 1.4: Two-lobe structure for the case with no interstellar magnetic field (Opher, 2015)

Comet-like Shape

The "comet-like" shape of the heliosphere is the most-accepted shape of the heliosphere. When the SW plasma flowing in the direction of LISM is deflect in the heliotail direction a "comet-like" structure of the heliosphere is formed (Pogorelov et al., 2015; Baranov and Malama, 1993; Zank and Pauls, 1996) that resembles the shapes seen in Figure (1.1) and Figure (1.2).

Bubble-like Shape

A different non-comet shape for the heliosphere is the so called "bubble" shaped structure of the heliosphere which is inferred from high energy ENAs map observed by the Cassini/INCA (Dialynas et al., 2017) as shown in Figure (1.5). The authors argue that the quick response in 5-55 keV ENAs from the tail direction indicate that it is very short. Others have pointed out that the ENA source region containing 5-55keV PUI is likely short, but this does not necessitate a short heliotail.

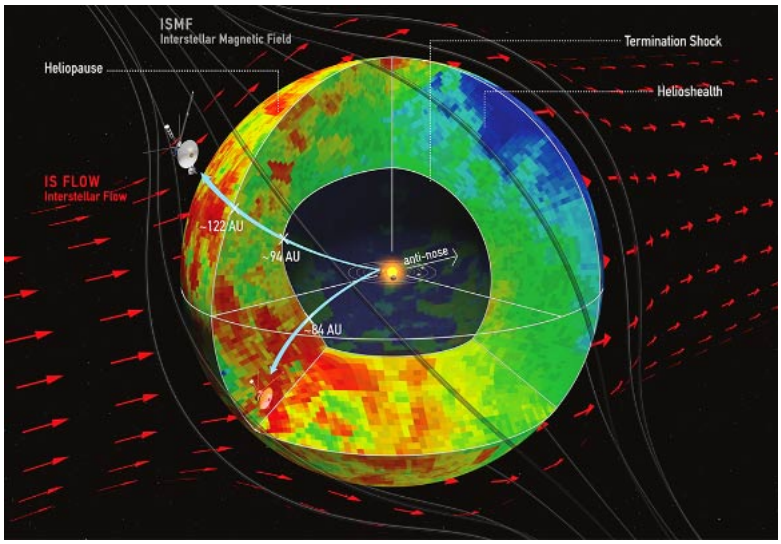

Figure 1.5: Bubble shape structure for the case with large interstellar magnetic field (Dialynas et al., 2017)

Most Convincing Shape Of The Heliosphere

A comet-like heliosphere is inferred by the remote measurement of ENAs by the Interstellar Boundary Explorer (IBEX). Analysis of ENAs produced by a time dependent simulation (Pogorelov et al., 2017) shows two lobes in northern and southern

hemisphere close to the heliotail. These are due to the fast SW present in the region above and below the ecliptic plane. Therefore, comet-like shape is the most convincing and is in agreement with the Zirnstein simulation. Hence, we follow comet-like structure of the heliosphere.

CHAPTER 2

PARKER'S MODEL

2.1 Parker's Model

To understand the heliospheric structure, we must know the properties of the solar wind at large distances from the Sun and it's extension in space and interaction with the interstellar medium. Parker (Parker, 1958, 1960a,b) developed a model of the SW based on continual hydrodynamic expansion rather than "corpuscular radiation". In general, the flow of SW is highly irregular. To simplify the problem we assume the outflow of gas is radial with spherical symmetry. The temperature of the stellar wind must be low due to it's expansion and thus the flow has a high Mach number. The stellar wind is supersonic in nature and undergoes a shock transition which is of a collisionless type where it becomes subsonic. Therefore, the Rankine - Hugoniot relations are

$$\rho_2 v_2 = \rho_1 v_1 \tag{2.1}$$

$$p_2 + \rho_2 v_2^2 = p_1 + \rho_1 v_1^2 \tag{2.2}$$

$$\frac{\gamma p_2}{(\gamma - 1)\rho_2} + \frac{1}{2} v_2^2 = \frac{\gamma p_1}{(\gamma - 1)\rho_1} + \frac{1}{2} v_1^2 \tag{2.3}$$

Where ρv is the mass that crosses a unite area in unit time , $(\rho v)v$ is the rate at which momentum is transported across a unit surface area, while p is the force acting on that area and γ is adiabatic index. Subscript 1 and 2 are for upstream and downstream of the shock.

In 1963, Parker proposed a model (Parker, 1963), assuming the flow downstream of the TS and LISM is incompressible and irrotational and also distance to the TS is very small compared to length scale of the heliopause. The model is as shown in Figure (2.1).

In the Parker model, plasma flow in the heliosphere is described by the set of fluid equations. The equation of motion is given by

$$\rho\left(\frac{d\mathbf{u}}{dt}\right) = -\nabla \mathrm{p} + \mathbf{j} \times \mathbf{B} + \mathbf{F}, \tag{2.4}$$

where $\mathbf{u}$ is the SW flow velocity, p is the plasma pressure, $-\nabla$p is the pressure gradient, $\mathbf{j} \times \mathbf{B}$ is the Lorentz force per unit volume and $\mathbf{F}$ is the external force.
The continuity equation

$$\frac{\partial n}{\partial t} + \nabla \cdot (n\mathbf{u}) = 0. \tag{2.5}$$

In a steady state, Equation (2.5) becomes

$$\nabla \cdot (\rho \mathbf{u}) = 0, \tag{2.6}$$

where $\rho = mn$ is the mass density of the plasma.

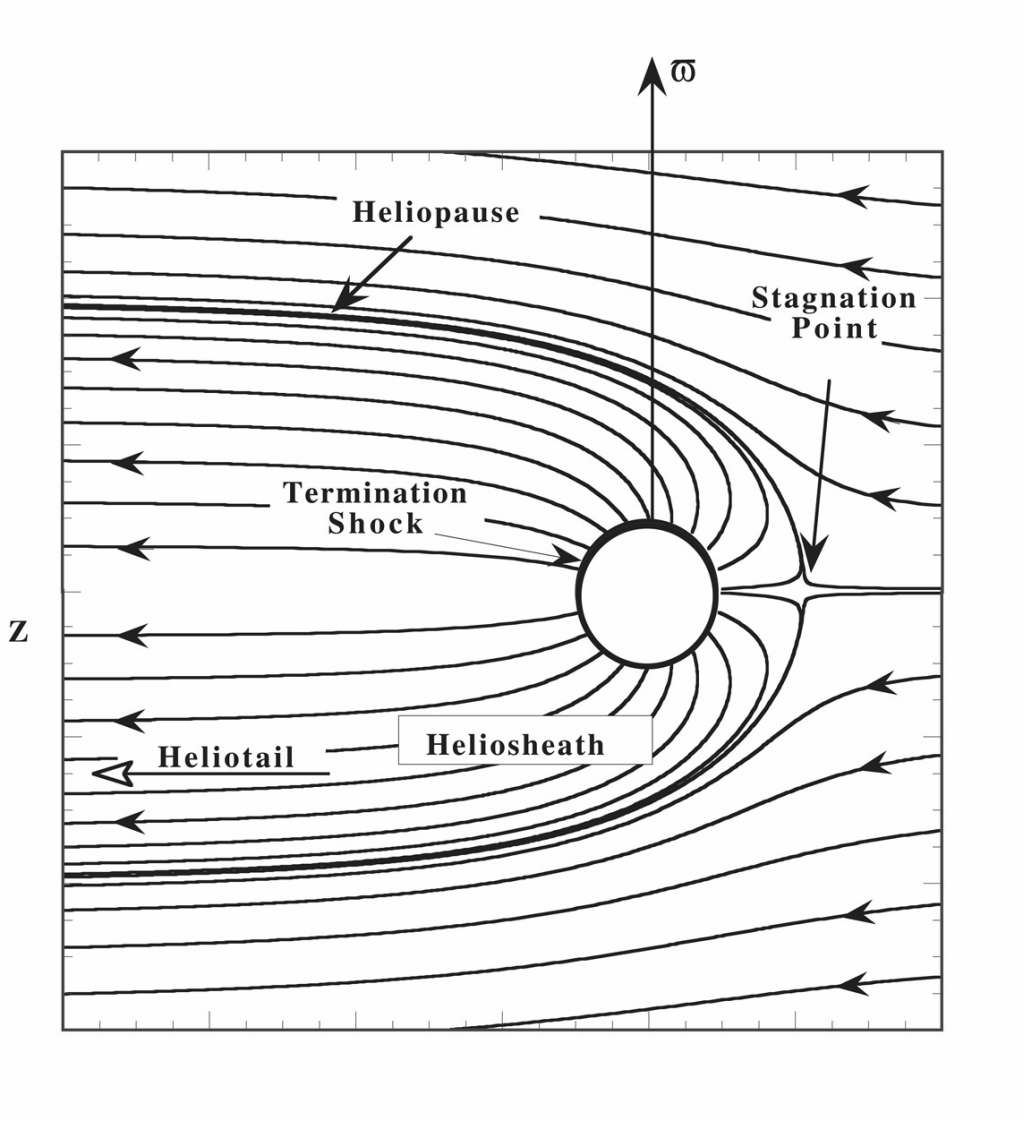

Figure 2.1: streamline plot for the irrotational flow. The flow is symmetric about heliotail (Suess and Nerney, 1991)

Assuming the plasma flow is incompressible i.e. density of a fluid is not affected by changes in the pressure ($\rho = constant$) (Batchelor, 2000) and the flow velocity has a zero divergence

$$\rho \nabla \cdot \mathbf{u} = 0, \tag{2.7}$$

$$\nabla \cdot \mathbf{u} = 0, \tag{2.8}$$

The assumption of irrotational plasma flow implies that there is no net rotation in the plasma flow and it is axisymmetric i.e.

$$\nabla \times \mathbf{u} = 0 \tag{2.9}$$

so the plasma flow velocity can be written as negative gradient of a scalar potential

$$\mathbf{u} = -\nabla\Phi, \tag{2.10}$$

where Φ is called a scalar potential for the flow velocity.

Combining Equations (2.8) and (2.10), we have

$$\nabla^2\Phi = 0 \tag{2.11}$$

This is Laplace's equation for the scalar potential of the plasma flow velocity.

2.2 Potential Flow Speed

Solution of Equation (2.11) can be written in terms of axisymmetric scalar potential as (Parker, 1961)

$$\Phi_1 = \frac{A}{r} + Br\cos\theta \tag{2.12}$$

Where the first on the right term describes the flow from a point source which is

radially outward and second term describes flow from LISM along z direction with $\nabla^2\Phi_1 = 0$.

When we add charge exchange term to the model, charge-exchange affects energy and momentum of SW plasma leading plasma to stagnation at finite distance (Khabibrakhmanov et al., 1996; Zirnstein and McComas, 2015). We assume

$$\nabla \cdot \mathbf{u} = -\frac{\nu_{ex}}{2\gamma}, \tag{2.13}$$

where $\nu_{ex} = n_H \sigma v_r$ is the rate of charge - exchange for protons in the ISH, n_H is hydrogen density, σ is charge-exchange cross section, v_r is relative velocity between interacting particles given by

$$v_r = \sqrt{\frac{2E_r}{m}}, \tag{2.14}$$

which is constant for given value of E_r and $\gamma = \frac{5}{3}$ is adiabatic index.

And thus we have Poisson's equation for the potential as

$$\nabla^2\Phi_2 = \frac{\nu_{ex}}{2\gamma}. \tag{2.15}$$

The flow is axisymmetric, and if ν_{ex} is dependent on r and θ it can be solved in terms of Legendre polynomials $p_k(\cos\theta)$ as

$$\frac{\nu_{ex}}{2\gamma} = \sum_{k=0}^{\infty} a_k(r) p_k(\cos\theta), \tag{2.16}$$

where,

$$a_k(r) = \left(k + \frac{1}{2}\right) \frac{\nu_{ex}}{2\gamma} \int_{-1}^{1} p_k(x)dx. \tag{2.17}$$

Also, we can express $\Phi_2(r, \theta)$ as

$$\Phi_2(r, \theta) = \sum_{k=0}^{\infty} \Phi_{2k}(r) p_k(\cos\theta). \tag{2.18}$$

Subtituting (2.16), (2.17) and (2.18) in Equation (2.15)

$$\nabla^2 \sum_{k=0}^{\infty} \Phi_{2k}(r) p_k(\cos\theta) = \sum_{k=0}^{\infty} a_k(r) p_k(\cos\theta). \tag{2.19}$$

For the expansion coefficient $\Phi_{2k}(r)$

$$\frac{1}{r^2}\frac{\partial}{\partial r}\left(r^2 \frac{\partial \Phi_{2k}(r)}{\partial r}\right) - \frac{k(k+1)}{r^2}\Phi_{2k}(r) = a_k(r). \tag{2.20}$$

For simplicity we assume ν_{ex} is constant everywhere and taking only zeroth-order term (k = 0) and comparing both sides

$$\frac{1}{r^2}\frac{\partial}{\partial r}\left(r^2 \frac{\partial \Phi_2(r)}{\partial r}\right) = a_0(r), \tag{2.21}$$

substituting the value of $a_0(k)$ from Equation (2.17)

$$\frac{1}{r^2}\frac{\partial}{\partial r}\left(r^2 \frac{\partial \Phi_2(r)}{\partial r}\right) = \frac{1}{2}\frac{\nu_{ex}}{2\gamma} \int_{-1}^{1} p_0(x)dx, \tag{2.22}$$

On further solving

$$\frac{1}{r^2}\frac{\partial}{\partial r}\left(r^2\frac{\partial\Phi_2(r)}{\partial r}\right) = \frac{\nu_{ex}}{4\gamma}(2), \tag{2.23}$$

$$\frac{\partial}{\partial r}\left(r^2\frac{\partial\Phi_2(r)}{\partial r}\right) = \frac{\nu_{ex}}{2\gamma}r^2, \tag{2.24}$$

On integrating we obtain

$$r^2\frac{\partial\Phi_2(r)}{\partial r} = \frac{\nu_{ex}}{2\gamma}\frac{r^3}{3} + C, \tag{2.25}$$

Where C is integration constant. This leads to

$$\frac{\partial\Phi_2(r)}{\partial r} = \frac{\nu_{ex}}{6\gamma}r + \frac{C}{r^2}, \tag{2.26}$$

Integrating this one more time gives

$$\Phi_2(r) = \frac{\nu_{ex}}{6\gamma}\frac{r^2}{2} - \frac{C}{r} + D, \tag{2.27}$$

$$\Phi_2(r) = \frac{\nu_{ex}}{12\gamma}r^2 - \frac{C}{r} + D, \tag{2.28}$$

Therefore total potential Φ is

$$\Phi = \Phi_1 + \Phi_2 \tag{2.29}$$

Substituting the values of Φ_1 and Φ_2 yields

$$\Phi = \frac{A}{r} + Br\cos\theta + \frac{\nu_{ex}}{12\gamma}r^2 - \frac{C}{r} + D, \tag{2.30}$$

which can be written as

$$\Phi = \frac{A-C}{r} + Br\cos\theta + \frac{\nu_{ex}}{12\gamma}r^2 + D. \tag{2.31}$$

The flow velocity in spherical coordinates is given by

$$u_r = -\frac{\partial\Phi}{\partial r} = \frac{A-C}{r^2} - B\cos\theta \ - \frac{\nu_{ex}}{6\gamma}r, \tag{2.32}$$

$$u_\theta = -\frac{1}{r}\frac{\partial\Phi}{\partial\theta} = B\sin\theta, \tag{2.33}$$

and $u_\phi = 0$, i.e. the axisymmetric flow.

Constants A, B and C in the above equation for velocity are determined with the help of boundary conditions. Due to the charge-exchange term radial velocity becomes infinite at very large distances (see Equation (2.32)). Because we are interested in the flow speed inside IHS, we choose the boundary condition at large but finite distance. Therefore (a) For $r = 1000\text{AU}, \theta = 0$

$$u(r = 1000\text{AU}, \theta = 0) = -\text{u}_{1000\text{AU}}, \tag{2.34}$$

$$\rightarrow u_r \equiv -B - \frac{\nu_{ex}}{6\gamma}(1000\text{AU}) = -\text{u}_{1000\text{AU}}, \tag{2.35}$$

Here, the term $\frac{A-C}{1000^2}$ is neglected (very small value).

$$\rightarrow B = u_{1000\text{AU}} - \frac{\nu_{ex}}{6\gamma} 1000\text{AU} = u_B. \tag{2.36}$$

(b) For $r = R_{TS}, \theta = 0$

$$u(r = R_{TS}, \theta = 0) = u_{TS} \rightarrow A - C, \tag{2.37}$$

$$= \left(u_{TS} + u_B + \frac{\nu_{ex}}{6\gamma} R_{TS} \right) R_{TS}^2, \tag{2.38}$$

Using the values of constant (A - C) and B, u_r and u_θ becomes

$$u_r = \left(u_{TS} + u_B + \frac{\nu_{ex}}{6\gamma} R_{TS} \right) \left(\frac{R_{TS}}{r} \right)^2 - u_B \cos\theta - \frac{\nu_{ex}}{6\gamma} r \tag{2.39}$$

$$u_\theta = u_B \sin\theta \tag{2.40}$$

In cartesian coordinates above two equations can be written as

$$u_x = u_r \sin\theta + u_\theta \cos\theta \tag{2.41}$$

$$u_x = \left(u_{TS} + u_B + \frac{\nu_{ex}}{6\gamma} R_{TS} \right) \left(\frac{R_{TS}}{r} \right)^2 \frac{x}{r} - \frac{\nu_{ex}}{6\gamma} x \tag{2.42}$$

and

$$u_z = u_r \cos\theta - u_\theta \sin\theta \tag{2.43}$$

$$u_z = \left(u_{TS} + u_B + \frac{\nu_{ex}}{6\gamma} R_{TS}\right)\left(\frac{R_{TS}}{r}\right)^2 \frac{z}{r} - \frac{\nu_{ex}}{6\gamma} z - u_B \tag{2.44}$$

In the absence of charge-exchange the potential $\Phi_2 = 0$, and the expression for the components of velocity can be derived as

$$u_x = (u_{TS} + u_B)\left(\frac{R_{TS}}{r}\right)^2 \frac{x}{r} \tag{2.45}$$

and

$$u_z = (u_{TS} + u_B)\left(\frac{R_{TS}}{r}\right)^2 \frac{z}{r} - u_B \tag{2.46}$$

Here Equation (2.42) and Equation (2.44) are the derivative of position with respect to time in the presence of charge-exchange, and Equation (2.45) and Equation (2.46) are in the absence of charge-exchange. These equations are solved numerically using the Runge Kutta method for the streamlines of the potential flow throughout the SW-LISM interaction region.

CHAPTER 3

CHARGE EXCHANGE

3.1 Charge Exchange

Charge exchange is the process in which an ion interacts with a neutral atom which loses its electrons. This process plays a very important role in studies of the heliosphere. The ions thus produced are called pick-up ions (PUIs).

When fast moving SW rich in H^+ and He^{++} and also some heavier elements, collides with the cold neutral H - atom from interstellar space, charge exchange takes place. The SW ions becomes neutralized energetic neutral atoms (ENAs), and interstellar neutral becomes ionized and picked up by magnetic field of the SW forming PUIs and move outward with the SW (Vasyliunas and Siscoe, 1976; Isenberg, 1986). The charge exchange relation between protons and Hydrogen can be represented by following equation

$$H^+ + H \longrightarrow H + H^+ \tag{3.1}$$

This process is visualized in Figure (3.1).

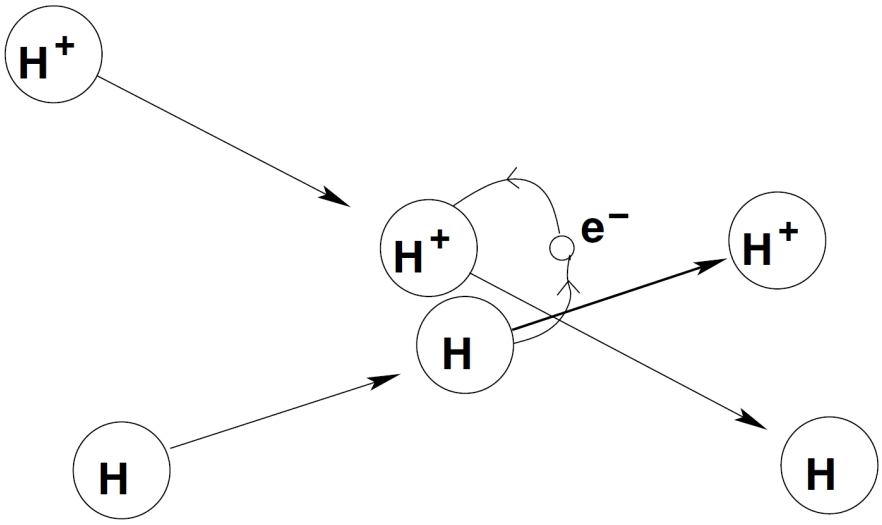

Figure 3.1: A cartoon of the charge-exchange process which couples the ionized plasma and neutral hydrogen gasses.

The charge-exchange cross section σ for $H - H^+$ interaction (Lindsay and Stebbings, 2005) is

$$\sigma(E_r) = (4.15 - 0.531 \ln(E_r))^2 \left(1 - \exp(-\frac{67.3}{E_r})\right)^{4.5} 10^{-16}\text{cm}^2, \tag{3.2}$$

with

$$E_r = \frac{1}{2} m v_r^2. \tag{3.3}$$

Here E_r is the kinetic energy of the charge-exchange interaction in keV and v_r is relative velocity between interacting particles.

The rate of charge exchange for protons is

$$\nu_{ex} = n_H \sigma v_r, \tag{3.4}$$

We calculate the rate of charge-exchange (ν_{ex}) using Equation (3.4). Where the value for σ is determined by Equation (3.2), value for v_r is determined by Equation (3.3) for the given value of E_r, and $n_H = 0.1$ cm^{-3}. After getting the value of ν_{ex}, we plug it into Equation (2.42) and Equation (2.44) to get the streamlines for potential flow as well as flow speed in the presence of charge-exchange.

CHAPTER 4

RESULTS AND DISCUSSIONS

From earlier chapters, we have seen that various models describe the shape of the heliosphere, SW - LISM interaction, and the shape was found to be spherical or bubbled or comet-like depending on the strength of the magnetic field. Among those models, we choose a simple 2D axially symmetric model of the heliosphere, in the presence of a very weak magnetic field which gives comet-like heliosphere. Even though our model is not very accurate, with certain simple modifications, we can reproduce comparable results to those obtained from 3D MHD-neutral simulation.

4.1 3D MHD-Neutral Heliospheric Simulation

In order to provide a reference heliosphere to which we can compare our analytic model, we take an ecliptic cut through the 3D steady state heliosphere obtained using the Huntsville MS-FLUKSS (Multi-Scale FLUid-Kinetic Simulation Suite) code (Pogorelov et al., 2009). In this simulation neutral particles are treated with a kinetic model and the flow of charged particles is treated with the ideal MHD equations. The LISM boundary conditions at 1000AU corresponding to the 3 μG LISM magnetic field magnitude are shown in Table (4.1) (Zirnstein et al., 2016).

Table 4.1: LISM Boundary Conditions at 1000 AU for $\mathbf{B}_\infty = 3\ \mu$ G

$\lvert\mathbf{B}_\infty\rvert$ (μ G)	3
$n_{p\infty}$ (cm^{-3})	0.09
$n_{H\infty}$ (cm^{-3})	0.154
V_∞ $(\frac{km}{s})$	25.4
T_∞ (k)	7500

An ecliptic cut through this 3D heliospheric simulation is shown in Figure (4.1).

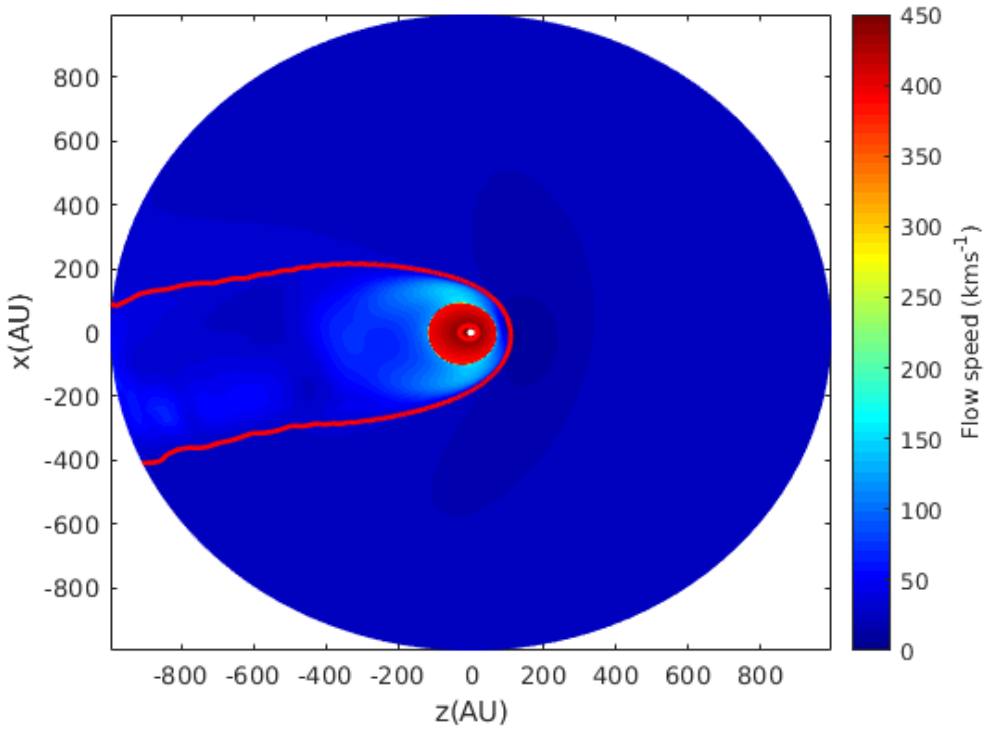

Figure 4.1: Cut through the 3D MHD-Neutral Simulation model for the heliosphere in the ecliptic plane. Red curve shows the location of heliopause corresponding to temperature 50,000 K and the background color represents the plasma flow speed.

4.2 Chi-Square Analysis

To determine how good our model is with respect to the 3D simulation result, we perform χ^2 analysis of the flow speed between two models. For χ^2 analysis, we calculate the value of χ^2 for every point inside the IHS using the formula

$$\chi_i^2 = (\frac{V_i - u_i}{\sigma_i})^2, \tag{4.1}$$

where i stands for a point in the IHS, V_i is the magnitude of flow speed in km/s from 3D simulation, u_i is the magnitude of flow speed in km/s from 2D model, and σ_i is error in the data, which comes from the simulation in this case, and it's value is assumed to be 1 km/s. The value of χ^2 simply means the relative difference between 2D flow speed and speed obtained from 3D simulation. Note that because $\sigma \equiv 1$ the magnitude of χ^2 we calculated will likely be very different from unity which is generally expected for a good fit.

In the following section we apply this analysis to compare the relative flow speed between 2D and 3D model and try to improve the 2D heliospheric model.

4.3 2D Heliospheric Model By Zirnstein And It's Comparison With The 3D Simulation

Zirnstein (Zirnstein and McComas, 2015), describes the 2D heliospheric model given by Parker in 1961, in the presence of charge-exchange. For this, authors choose 1 keV protons for the charge-exchange term, with $u_{TS} = 150$ km/s, $R_{TS} = 90$ AU

(see section 2.2). The resulting SW-LISM interaction is shown in Figure (4.2).

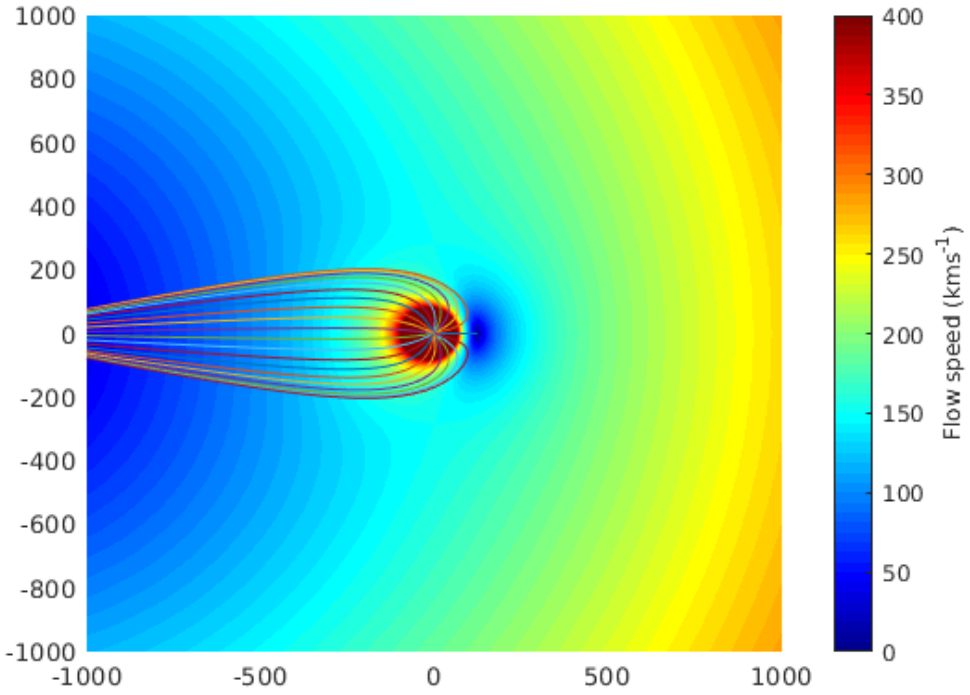

Figure 4.2: Zirnstein 2D heliospheric model for $u_{TS} = 150$ km/s, $R_{TS} = 90$ AU and charge-exchange interaction energy for proton $E_r = 1$ keV showing the plasma flow speed in km/s. Streamline of SW flow map out the heliosphere and heliotail (Zirnstein and McComas, 2015)

To evaluate the accuracy of the potential flow model, we compare the 2D flow speed of the SW with the 3D simulation in the region between the TS and HP and also calculated the χ^2 value to see the difference between the simulation and the simple 2D model (see Equation (4.1)). This calculation is done with and without the

charge-exchange term using Equation (2.42), Equation (2.42) and Equation (2.45), Equation (2.45) as shown in Figure (4.4) and Figure (4.3) respectively. From this comparison, we can see that even though the potential flow model seems quite good to represent the plasma flow streamline in the IHS, the values for the χ^2 are very high.

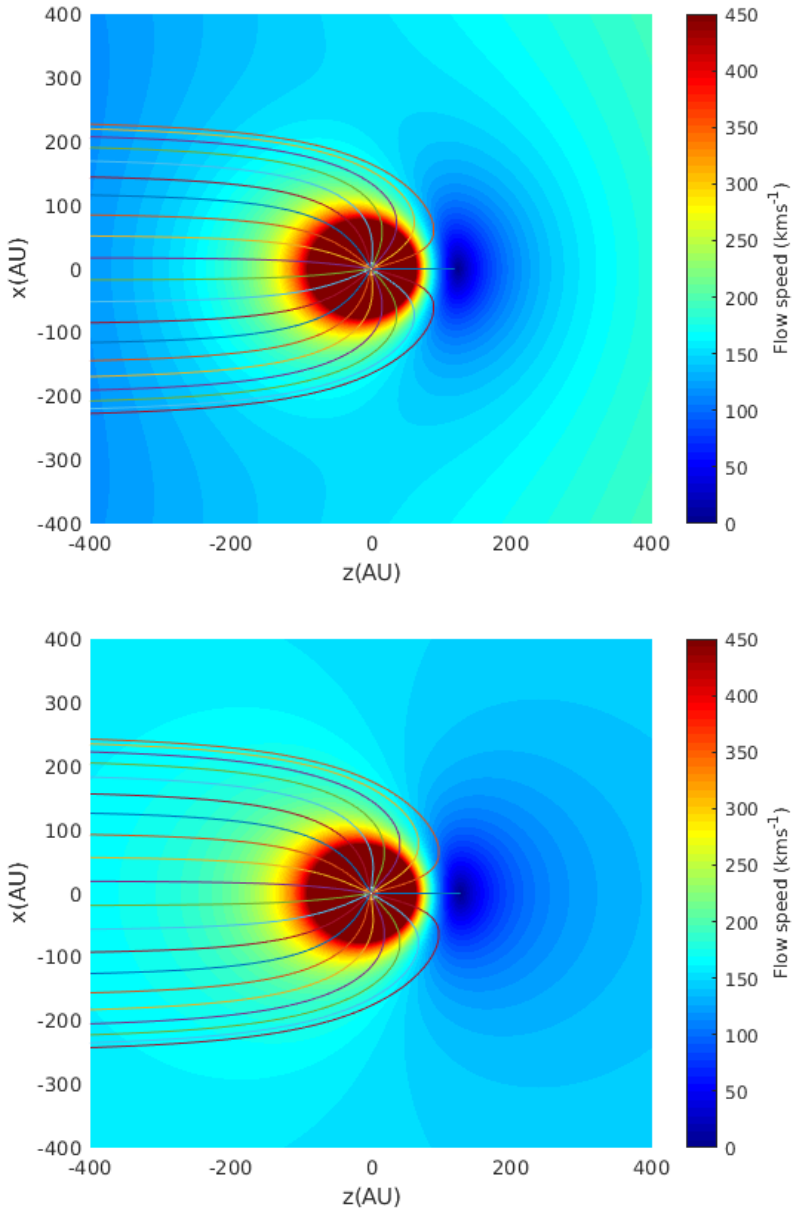

Figure 4.3: Flow speed with Zirnstein parameters $u_{TS} = 150$ km/s, $R_{TS} = 90$ AU and $E_r = 1$ keV in the presence (top) and absence (bottom) of charge-exchange.

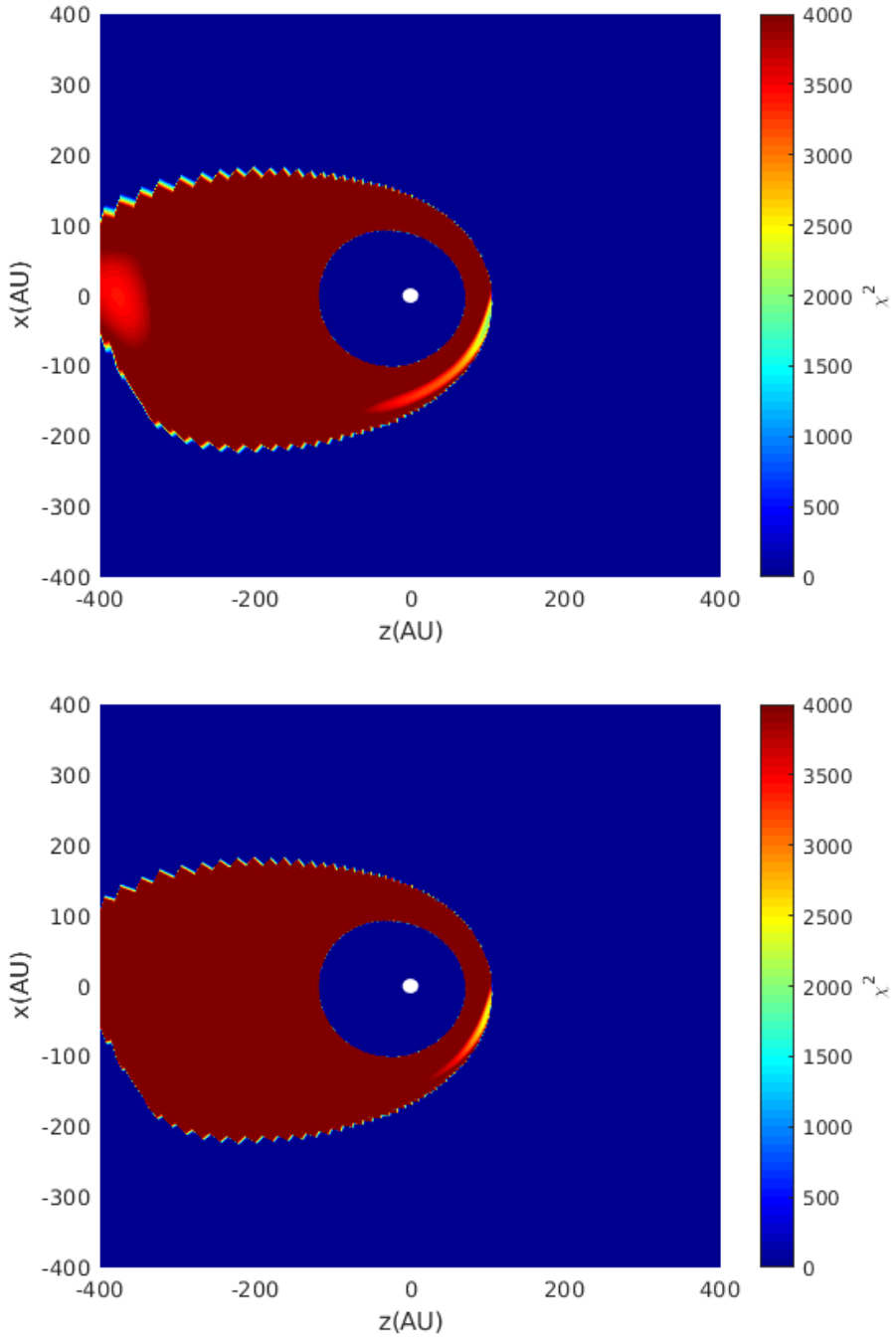

Figure 4.4: χ^2 value with Zirnstein parameters $u_{TS} = 150$ km/s, $R_{TS} = 90$ AU and $E_r = 1$ keV in the presence (top) and absence (bottom) of charge-exchange in the IHS region.

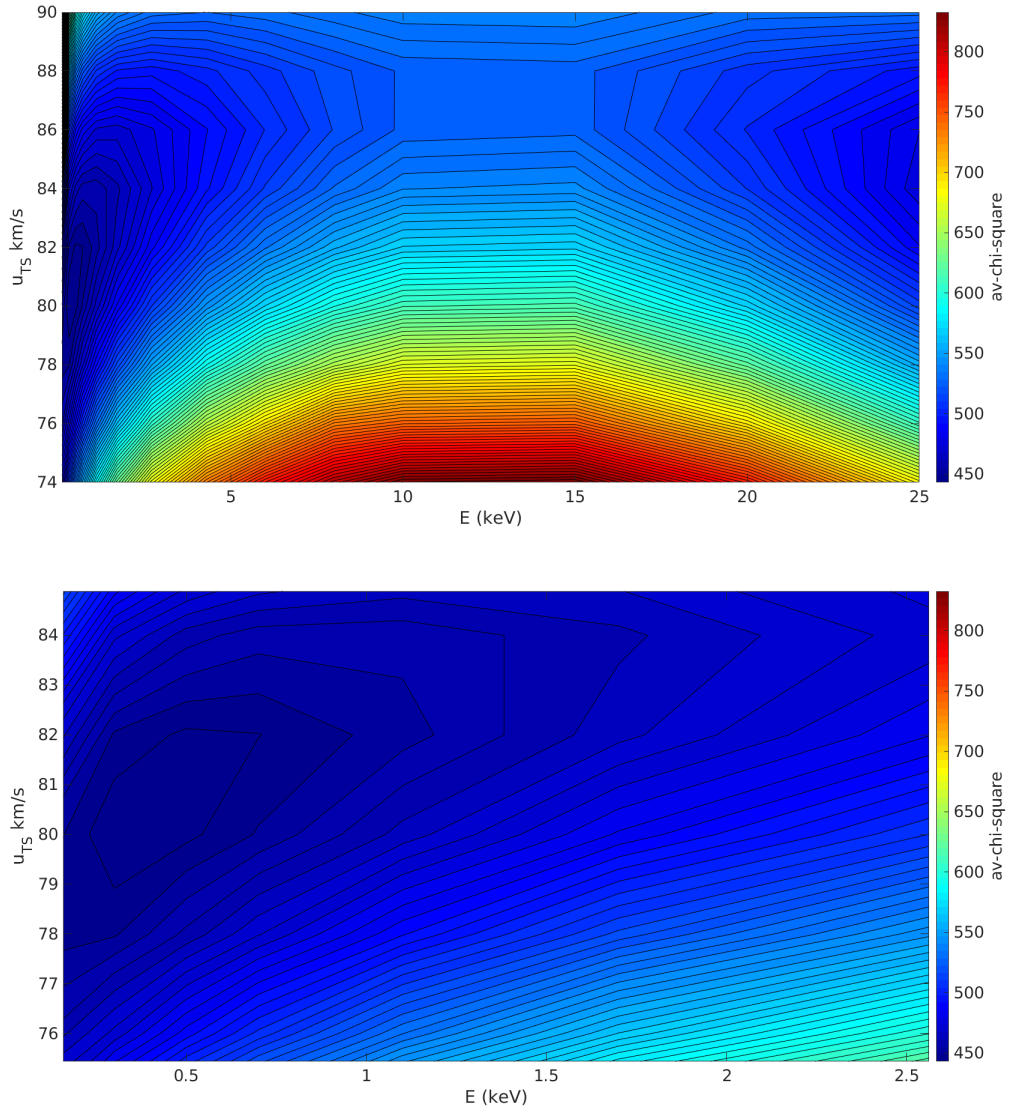

Figure 4.5: Chi-square values calculated for different velocity and energy range. Top figure shows the contour for the minimum chi-square value for energy 0.1-25 keV and speed u_{TS} 74-90 km/s and bottom figure shows the zoom in plot for the contour

4.3.1 Chi-Square Analysis For The Magnitude Of Velocity

Having established that the parameters chosen by Zirnstein do not provide a good fit to the simulation, we performed a χ^2 analysis using the magnitude of the velocity in the inner heliosheath.

Since we know that the charge-exchange term results in zero flow velocity at a finite distance down the heliotail, we restricted our analysis to a region defined by the temperature in the simulation being greater than 1,000,000K. This region includes the nose and flanks of the heliosheath and extends about 400 AU in the tailward direction.

For each simulation grid-cell, we compute the value of χ^2 according to Equation (4.1), and then average them over the region of interest (i.e. T > 1,000,000k). For the analysis, we fixed $R_{TS} = 84$ AU, which provide a reasonable agreement with the simulation, on average. We then varied u_{TS}, the flow speed of the SW and energy E_r used in the charge-exchange source term and computed the average χ^2 value within the region for which T > 1,000,000 for each resulting model. We constructed a 9×14 grid cell such that $74 \leq u_{TS} \leq 90$ km/s and $0.1 \leq \mathrm{E} \leq 25$ keV and calculated the χ^2 value for each gris cell. The plot thus we obtained has closed contour which corresponds to χ^2 minimization as shown in first plot of Figure (4.5).

Based on chi-square analysis we modified the Zirnstein model by changing parameters from $U_{TS} = 150$ km/s to $U_{TS} = 81$ km/s, $R_{TS} = 90$ AU to $R_{TS} = 84$ AU ,and proton energy from 1 keV to 0.4 keV for the charge-exchange term. We plot for 2D heliospheric model with modified parameter and it's comparison with 3D heliospheric model is as shown in Figure (4.6) and Figure (4.7).

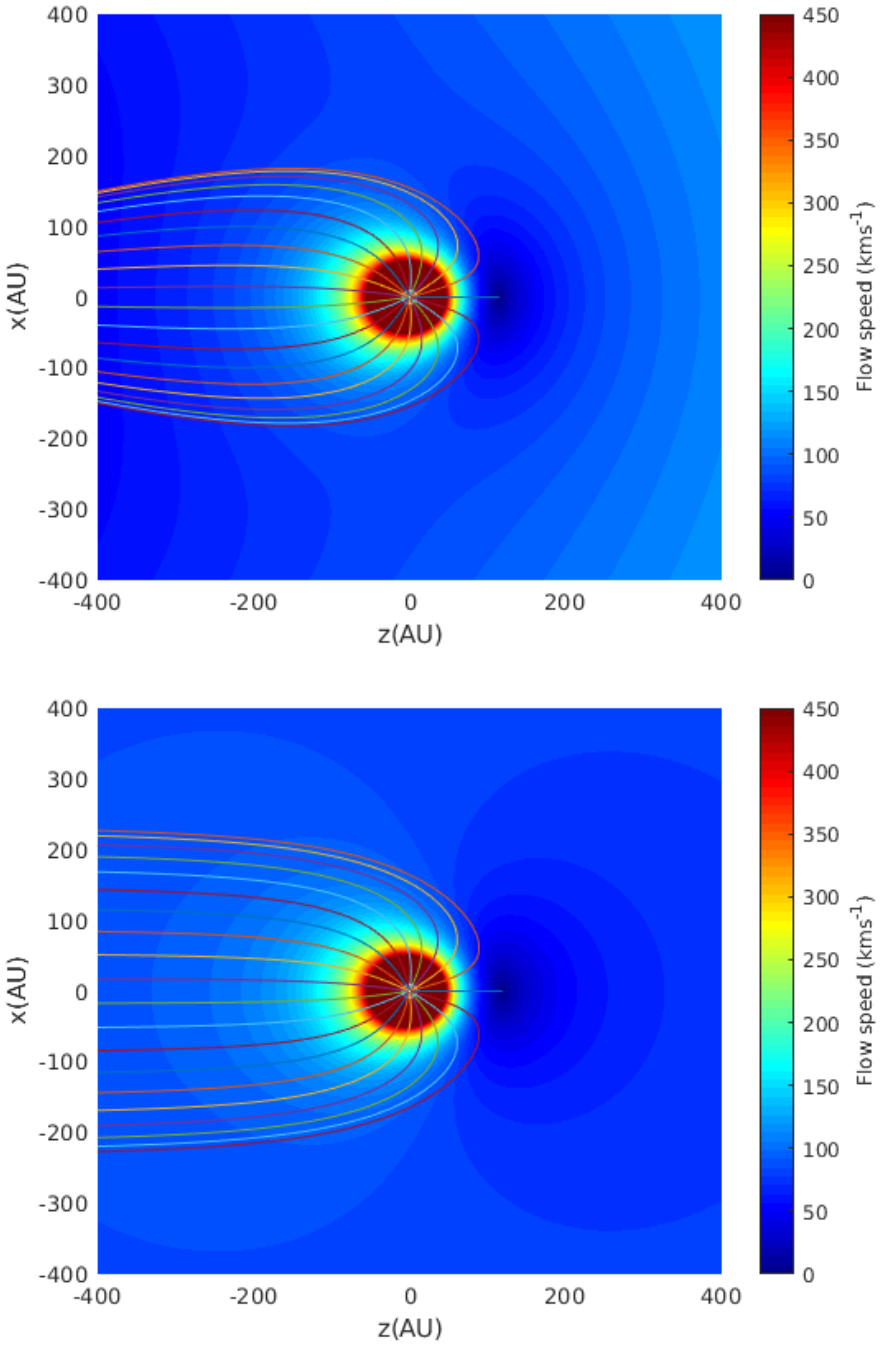

Figure 4.6: Flow speed with parameters $u_{TS} = 81$ km/s, $R_{TS} = 84$ AU and $E_r = 0.4$ keV in the presence (top) and absence (bottom) of charge-exchange.

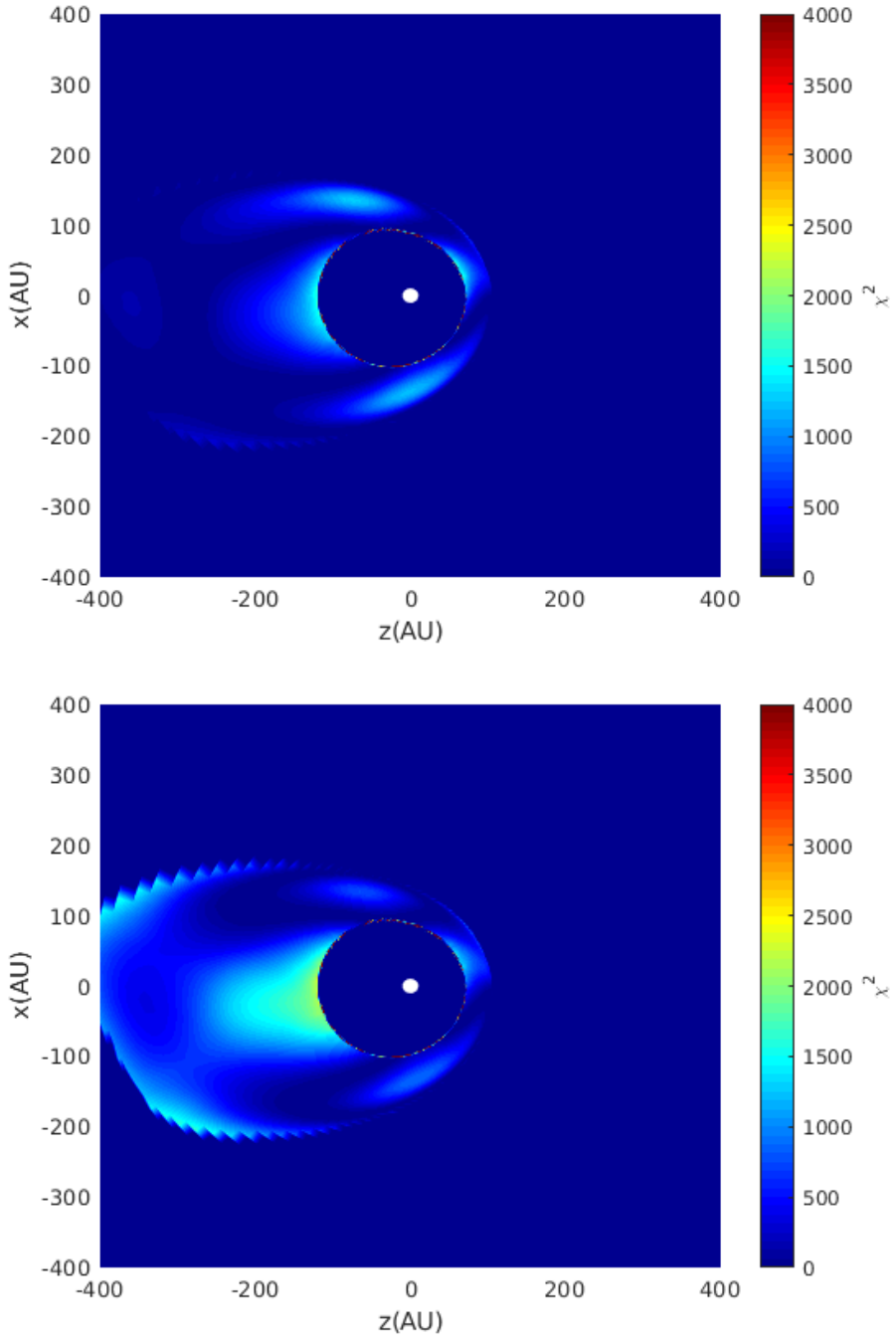

Figure 4.7: χ^2 value with parameters $u_{TS} = 81$ km/s, $R_{TS} = 84$ AU and $E_r = 0.4$ keV in the presence (top) and absence (bottom) of charge-exchange in the IHS region.

From these plots we can see that the modified Zirstein flow model agrees much more closely with the simulation than the Zirnstein flow model, and also that the χ^2 value is significantly reduced.

4.3.2 Chi-Square Analysis For The Velocity Component

In the previous section we used the velocity magnitude to derive a χ^2 minimization for the model parameters u_{TS} and E_r. In this section we check to see whether the resulting velocity components have a similar error to the magnitude. For this, we calculate the relative difference in x and z the component of 2D flow speed and 3D flow speed by calculating the chi-square value. Plots are as shown in Figure (4.8) for z-component (top) and x-component (bottom) of velocity in the presence of charge-exchange term. From these plots we observe that the chi-square value in the IHS region is similar to those we obtained while comparing the magnitude of flow speed of 2D and 3D heliospheric model. This indicates that our method of analyzing the velocity magnitude is sufficient to provide a good estimate of the velocity components.

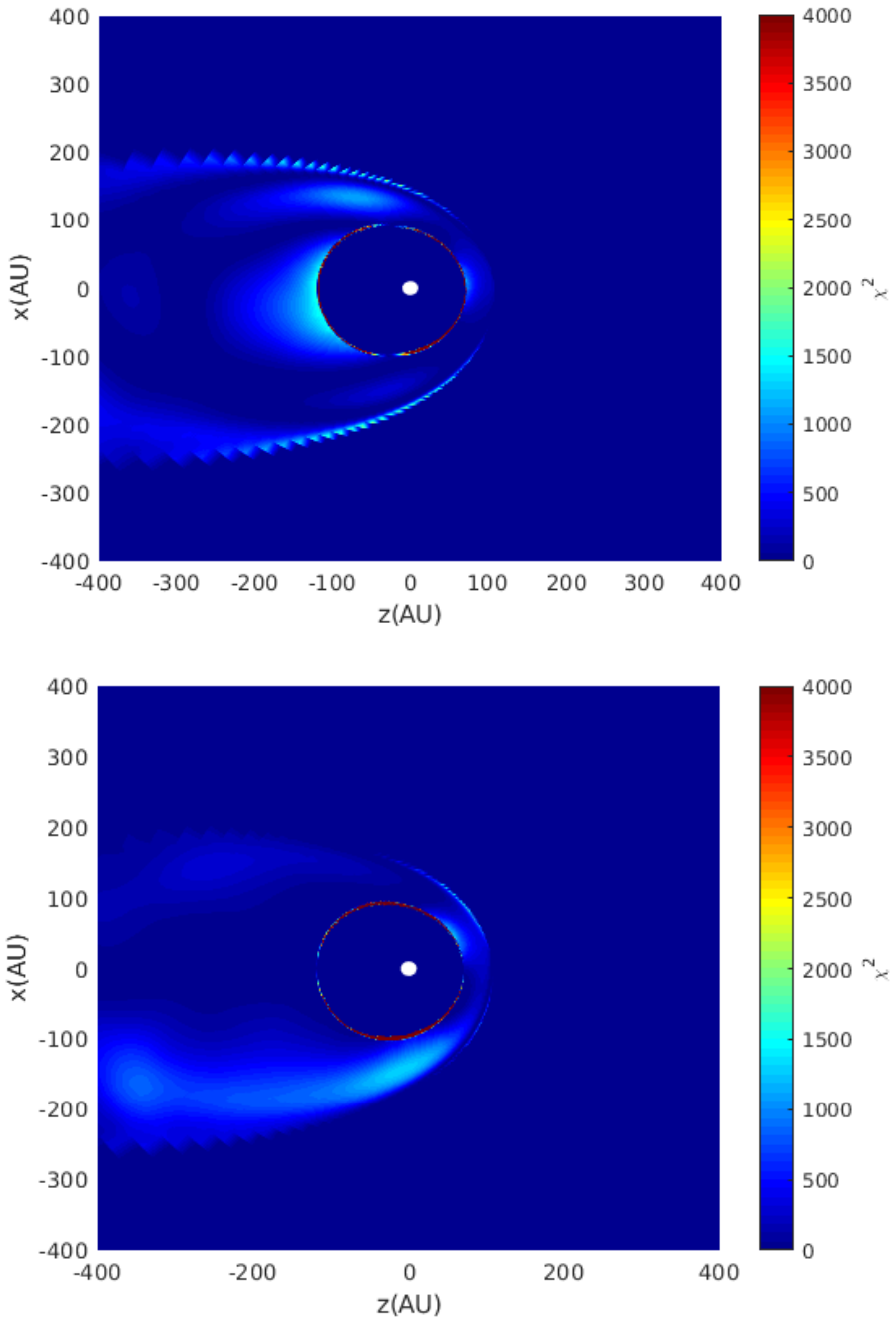

Figure 4.8: Chi-square analysis for relative difference between the z-component(top) and x- component(bottom) of velocity in the presence of charge-exchange with parameters $u_{TS} = 81$ km/s, $R_{TS} = 84$ AU and $E_r = 0.4$ keV.

4.4 Heliopause Location

Another important aspect of models of the heliosphere is the location of the heliopause. The heliosphere is the streamline that can be traced backward, starting at some point at a distance (e.g. 400 AU) in the heliotail direction, around to the stagnation point in front of the heliosphere. In our code, we achieve this using a bisection method. In this method, to find the position of the heliopause, we used bi-section method between two values of x, e.g., 175AU and 300AU for a fixed value of z (-400AU in our case) initially. To get streamlines, we use RK45 in the backward direction for a fixed value of z and points between 175AU and 300AU with some additional condition. The condition that we set to find the position for heliopause was if the streamline goes beyond z = 400 breaks it and set high value of x to mid value. Also if during the integration of the streamline, a new value of z is less than the previous value of z, set a lower value of x to mid value. We did this for a large number of iteration until we got a constant value of x. After getting the fixed value for x, we plot to streamline by taking that value and value of z, which is our heliopause. In the 3D simulation, we find the approximate location of the heliopause by plotting a temperature counter for the temperature of 50,000 K.

In this section, we compare the position of the heliopause given by the 3D MHD - neutral simulation, the Zirnstein model and the modified Zirnstein model as shown in Figure (4.9). From this figure, we observed that the modified Zirnstein model is in close approximation with 3D simulation result.

The asymmetry of the heliopause in 3D simulation result is due to the effects of the LISM magnetic field draping around the heliopause.

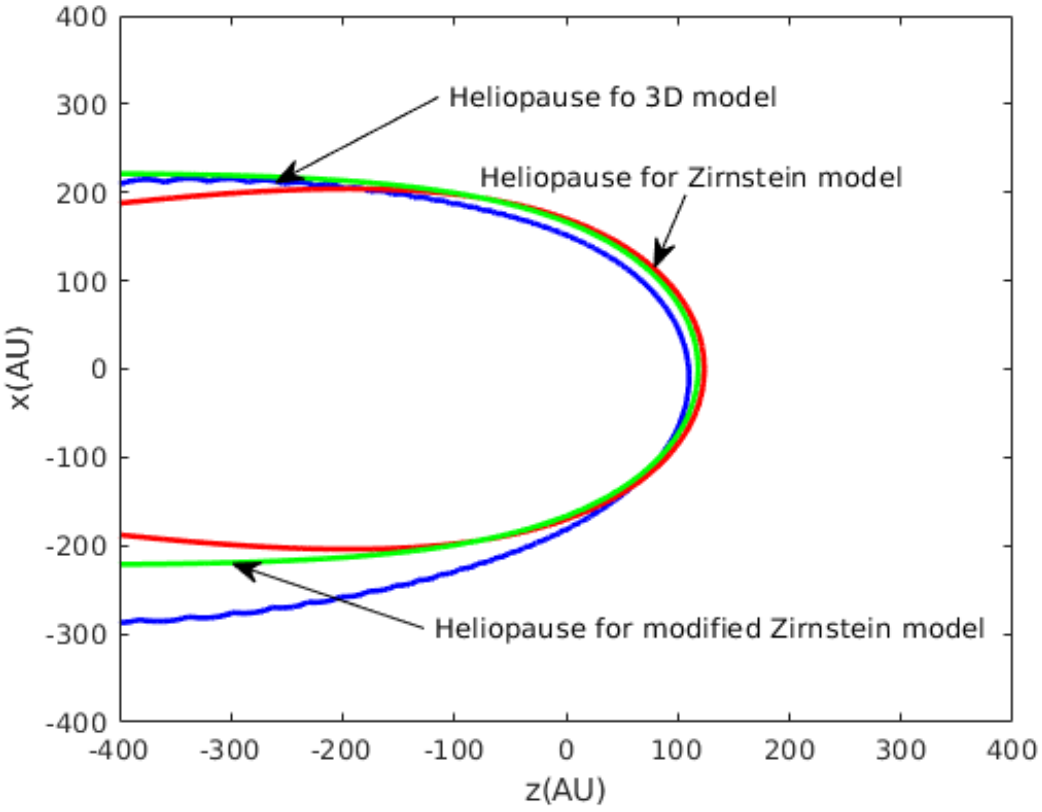

Figure 4.9: Position of Heliopause. Where blue curve shows heliopause for 3D simulation, red curve shows heliopause for Zirnstein model (u_{TS} = 150 km/s, R_{TS} = 90 AU, E = 1 keV) and green curve shows heliopause for modified Zirnstein parameters (u_{TS} = 81 km/s, R_{TS} = 84 AU, E = 0.4 keV)

CHAPTER 5

CONCLUSIONS

The heliosphere is believed to be a comet-like shaped structure, formed by the SW-LISM interaction. With limited data on the shape and structure of the heliosphere, scientists often turn to models to provide context for data. So many models describe the SW-LISM interaction, covering a wide range of sophistication. From these, we choose an elementary model given by Parker (1961) in the absence of a magnetic field, which was modified by Zirnstein (Zirnstein and McComas, 2015) by adding a charge-exchange term. Zirnstein took $u_{TS} = 150$ km/s, $R_{TS} = 90$ AU , and added a charge-exchange term based on 1 keV protons.

We took the ecliptic cut of the flow speed obtained from the 3D model as standard and compared 2D flow speed with this to see the accuracy of the model. In the Zirnstein model, the flow speed in IHS region in very high which is indicated by the high χ^2 value as shown in Figure (4.3) and Figure (4.4). In order to improve this model, we performed χ^2 analysis for flow speed u_{TS} and proton energy E_r used in charge-exchange term with a fixed value of distance to the TS, $R_{TS} = 84$ AU. This analysis gives us optimal values of flow speed u_{TS} and proton energy E_r as 81 km/s and 0.4 keV respectively. Using these values to modify the 2D heliospheric model and

plot 2D potential flow speed, we got the improved model which compares well with the 3D model as shown in Figure (4.6), and the χ^2 value is significantly reduced as shown in Figure (4.7).

The χ^2 analysis of the x- and z-component of the velocity in the IHS region in the presence of charge-exchange gives comparable χ^2 to the total magnitude of the velocity which indicates that the y-component of the velocity in the ecliptic region is almost negligible, and the flow can be assumed to be 2D flow as shown in Figure (4.8).

Finally, we plotted the heliopause for the Zirsntein model, our optimized model, and the 3D simulation. The variation in the location of the heliopause from the 3D simulation reflects the fact that heliopause is not symmetric and affected by the draping of the interstellar magnetic field around the heliopause. As such, no axially symmetric flow model will be able to reproduce it exactly. However, the optimized model does provide a qualitatively better fit.

Overall we conclude that a simple potential flow model could be used over a limited region in the heliosheath if we are only interested in the plasma flow properties. For more sophisticated modeling of density, pressure, and magnetic field a 3D MHD-neutral based simulation is still preferred.

CHAPTER 6

APPENDIX A

Code For The Bisection Method

```
// code for bisection method

#include <cmath> // for sqrt()

#include <iostream>

#include <iomanip>

using namespace std;

// physical parameter

const double uTS = 150.0 / 1.496e+8;

const double uB  = uTS;

const double RTS = 90.0;

const int  nmax = 100;

const int imax = 2000000; // number of time steps

const double dt = 3000.0; // time step

const double gama = 5.0/3.0;

const double nu_ex = 7.5e-9;

double r;

void computeG(double x, double z, double &dx, double &dz)
```

```
{
  r = sqrt(x*x + z*z);
  dx = (uTS + uB + nu_ex * RTS / (6.0 * gama)) * (RTS / r) * (RTS / r )
  * x / r - nu_ex * x / (6.0 * gama) ;
  dz = -uB + (uTS + uB + nu_ex * RTS / (6.0 * gama)) * (RTS / r) * (RTS / r )
  * z / r - nu_ex * z / (6.0 * gama);
  // integrating BACKWARD
  dx = -dx;
  dz = -dz;
};
int main(void)
{
  double time[imax + 1], xtraj[imax + 1], ztraj[imax + 1];
  double t0, x0, z0, r0, x_0, x_1, x_2;
  double dx1, dz1, dx2, dz2, dx3,  dz3, dx4, dz4;
  double theta , x1, x2;
  int i, j;
  // initilizing the values
  x_1 = 150.0;
  x_2 = 300.0;
 // iteration for bisection method
   for (j =0; j <= nmax; j++){
     x_0 = 0.5 * (x_1 + x_2);
     xtraj[0] = x_0 ;
```

```
     ztraj[0] = -400.0;
     int niter = 0;
  // integrate in time
  //iteration for RK45 method
     for(i = 1; i <= imax; i++){
       time[0] = 0.0;
       t0 = time[i-1];
       x0 = xtraj[i-1];
       z0 = ztraj[i-1];
computeG(x0, z0, dx1, dz1);// k1
computeG(x0 + 0.5*dt*dx1, z0 + 0.5*dt*dz1, dx2, dz2);// k2;
computeG(x0 +  0.5*dt*dx2, z0 + 0.5*dt*dz2, dx3, dz3); //k3
        computeG(x0 + dt*dx3, z0 + dt*dz3, dx4, dz4); //k4
time[i] = time[i-1] + dt;
xtraj[i]  = xtraj[i-1]  + dt*(1.0 * dx1/6.0  + 1.0 *dx2/3.0 + 1.0*dx3/3.0
+ 1.0*dx4/6.0);
        ztraj[i]  = ztraj[i-1]  + dt*(1.0 * dz1/6.0  + 1.0 *dz2/3.0
        + 1.0*dz3/3.0+ 1.0*dz4/6.0);
   // breaking condition
      if(ztraj[i] > 400.0){
x_2 = x_0;
 break;
       }
       if(ztraj[i] < ztraj[i-1]){
```

```
       x_1 = x_0;
 break;
       };
      //  niter++;
      };
      cout << setw(25) << setprecision(16)<<x_0
   // << setw(20) << setprecision(10)<<xtraj[i]
   // << setw(20) << setprecision(10)<<ztraj[i]
  << endl;
      };


    return 0;
};
```

CHAPTER 7

APPENDIX B

Code For Chi-Square Analysis

```
clear;

close all;

%-code for the chi-square test in IHS region------------------------------

B_3 = load('B_LISM3muG_slice.dat');   % Data from an ecliptic cut of 3D simulation

r = B_3(:,1);                         % distance in AU

theta = B_3(:,2);                     % angle in radian

T = B_3(:,7);                         % temperature in kelvin

vz = B_3(:,4);                        % z-component of velocity in km/s

vx = B_3(:,5);                        % x-component of velocity in km/s

vy = B_3(:,6);                        % y-component of velocity in km/s

% for 2d potential flow calculation

%%%%%%%%%%%%%%%%%%%%%%%%%%%%%%%%%%%%%%%%%%%%%%%%%%%%%%%%%%%%%%%%%%%%%%%%%%%

%-------------------------------------------------------------------------

uTS = 81.0  / 1.496e+8;         %  velocity at TS in AU/s

uB  = uTS;

RTS = 84.0;                    % diatsnce at TS in AU
```

```
gama = 5.0/3.0;

m_H = 1.6737236 *1e-27;        % mass of Hydrogen in kg

E = 0.4;                       % proton energy always in keV

 % cross section in cm^2

sigma_ex = (4.15 - 0.531*log(E))^2 * (1- exp(-67.3/E))^4.5 *1e-16;

n_H = 0.1;                     % hydrogen density in cm^-3

u_rel = sqrt(2*E*1e+3*1.6e-19 /m_H)*100; % relative velocity in cm/s

nu_ex = n_H * sigma_ex * u_rel;  % rate of charge exchange in per second

%%% reshaping

R = reshape(r,[118,380]);

THETA = reshape(theta,[118,380]);

Tmp = reshape(T,[118,380]);

%%% initiliting the matrix

x = zeros(118,380);

z = zeros(118,380);

radius = zeros(118,380);

ur = zeros(118,380);

utheta = zeros(118,380);

ux = zeros(118,380);

uz = zeros(118,380);

u = zeros(118,380);

%-------------------------------------------------------------------------------------

for i = 1:118

    for j = 1:380
```

```
        x(i,j) = R(i,j) * sin(THETA(i,j));

        z(i,j) = R(i,j) * cos(THETA(i,j));


        radius(i,j) =  sqrt(x(i,j) * x(i,j) + z(i,j) * z(i,j));


        % with charge exchange term
         ux(i,j) = (uTS + uB + (nu_ex * RTS / 6.0 / gama)) * (RTS / radius(i,j))^2
         * x(i,j)/radius(i,j) - (nu_ex * x(i,j) / 6.0 / gama);
         uz(i,j) = (uTS + uB + (nu_ex * RTS / 6.0 / gama)) * (RTS / radius(i,j))^2
         * z(i,j)/radius(i,j) - (nu_ex * z(i,j) / 6.0 / gama) - uB;


      %  without charge exchange term
%          ux(i,j) = (uTS + uB) * (RTS / radius(i,j))^2 * x(i,j)/radius(i,j);
%          uz(i,j) = (uTS + uB) * (RTS / radius(i,j))^2 * z(i,j)/radius(i,j) - uB;


       u(i,j)  =  sqrt(ux(i,j) * ux(i,j) + uz(i,j) * uz(i,j))*1.496e+8;
    end
end


x(118+1,:) = x(1,:);
z(118+1,:) = z(1,:);
u(118+1,:) = u(1,:);
Tmp(118+1,:) = Tmp(1,:);
% uz(118+1,:) = uz(1,:);
```

```
% ux(118+1,:) = ux(1,:);

% pcolor(z,x,u)

% shading interp;

% colormap jet

% caxis([0 450])

% h = colorbar;

% h.Label.String = 'Flow speed (kms^{-1})';

% hold on

%%% loading data for streamlines

% z1 = load('kk1.dat');

% x1 = load('ll1.dat');

% for k = 1:21

% plot(z1(k,:), x1(k,:))

% hold on1.496e+8

% end

% caxis([0 450])

 xlim([-400 400]),ylim([-400 400])

% xlabel('z(AU)'),ylabel('x(AU)')

% pause

% clf;

%%%%%%%%%%%%%%%%%%%%%%%%%%%%%%%%%%%%%%%%%%%%%%%%%%%%%%%%%%%%%%%%%%%%%%%%%%%%%%%

% IHS parameters from 3D ecliptic cut

v = sqrt(vx.^2 + vy.^2 + vz.^2);

V = reshape(v,[118,380]);
```

```
V(118+1,:) = V(1,:);

% identify IHS region with T > 1000,000

non_dof = 0; % # of grids with T < 1000,000

for i = 1:119

    for j = 1: 380

        if Tmp(i,j) < 1000000

            Tmp(i,j) = 0;

            u(i,j) = 0;

            V(i,j) = 0;

            uz(i,j) = 0;

            ux(i,j) = 0;

            non_dof = non_dof + 1;

        end

    end

end

pcolor(z,x,Tmp)

shading interp

colormap jet

h = colorbar;

h.Label.String = 'Temp (K)';

xlim([-400 400]),ylim([-400 400])

xlabel('z(AU)'),ylabel('x(AU)')

% pause

% clf;
```

```
%%%%%%%%%%%%%%%%%%%%%%%%%%%%%%%%%%%%%%%%%%%%%%%%%%%%%%%%%%%%%%%%%%%%%%%%%%%%%%%%
% chi_square value
chisquare = zeros(119,380);
for i = 1:119
    for j = 1:380
        chisquare(i,j) = (V(i,j) - u(i,j)).^2;
    end
end
avg_chi_square = sum(chisquare(:))/(119*380 - non_dof); % average chi-square
%plot of chi_square
% pcolor(z,x,chisquare)
% xlim([-400 400]),ylim([-400 400])
% shading interp
% colormap jet
% caxis([0 4000])
% c = colorbar;
% c.Label.String = '\chi^2';
 xlabel('z(AU)'), ylabel('x(AU)')
```

REFERENCES

Baranov, V. B. and Malama, Y. G. (1993). Model of the solar wind interaction with the local interstellar medium - Numerical solution of self-consistent problem. *Journal of Geophysical Research*, 98:15.

Batchelor, G. K. (2000). *An Introduction to Fluid Dynamics*.

Decker, R. B., Krimigis, S. M., Roelof, E. C., and Hill, M. E. (2008). Particle Acceleration at the Termination Shock: Voyager 1 and 2 Observations. In Li, G., Hu, Q., Verkhoglyadova, O., Zank, G. P., Lin, R. P., and Luhmann, J., editors, *American Institute of Physics Conference Series*, volume 1039 of *American Institute of Physics Conference Series*, pages 349–354.

Dessler, A. J. (1967). Solar Wind and Interplanetary Magnetic Field. *Reviews of Geophysics and Space Physics*, 5:1–41.

Dialynas, K., Krimigis, S. M., Mitchell, D. G., Decker, R. B., and Roelof, E. C. (2017). The bubble-like shape of the heliosphere observed by Voyager and Cassini. *Nature Astronomy*, 1:0115.

Florinski, V. (2009). Pickup Ion Acceleration at the Termination Shock and in the Heliosheath. *Space Science Reviews*, 143:111–124.

Gringauz, K. I., Kurt, V. G., Moroz, V. I., and Shklovskii, I. S. (1960). Ionized gas and high energy electrons in the vicinity of the earth and in the interplanetary space. In *Doklady Akademii Nauk*, volume 132, pages 1062–1065. Russian Academy of Sciences.

Heerikhuisen, J., Pogorelov, N. V., Florinski, V., and Zank, G. P. (2008). Modeling Kinetic Neutral Atoms in the Solar-Wind/Interstellar-Medium Interaction Region. In Pogorelov, N. V., Audit, E., and Zank, G. P., editors, *Numerical Modeling of Space Plasma Flows*, volume 385 of *Astronomical Society of the Pacific Conference Series*, page 204.

Heerikhuisen, J., Zirnstein, E. J., Funsten, H. O., Pogorelov, N. V., and Zank, G. P. (2014). The Effect of New Interstellar Medium Parameters on the Heliosphere and Energetic Neutral Atoms from the Interstellar Boundary. *The Astrophysical Journal*, 784:73.

Isenberg, P. A. (1986). Interaction of the solar wind with interstellar neutral hydrogen - Three-fluid model. *Journal of Geophysical Research*, 91:9965–9972.

Isenberg, P. A., Forbes, T. G., and Möbius, E. (2015). Draping of the Interstellar Magnetic Field over the Heliopause: a Passive Field Model. *The Astrophysical Journal*, 805:153.

Izmodenov, V. V. and Alexashov, D. (2005). Kinetic Vs Multi-Fluid Models of H Atoms in the Heliospheric Interface. In Fleck, B., Zurbuchen, T. H., and Lacoste, H., editors, *Solar Wind 11/SOHO 16, Connecting Sun and Heliosphere*, volume 592 of *ESA Special Publication*, page 355.

Kaiser, M. L., Kucera, T., Davila, J., Cyr, O. S., Guhathakurta, M., and Christian, E. (2008). The stereo mission: An introduction. *Space Science Reviews*, 136(1-4):5–16.

Khabibrakhmanov, I. K., Summers, D., Zank, G. P., and Pauls, H. L. (1996). Solar Wind Flow with Hydrogen Pickup. *The Astrophysical Journal*, 469:921.

Lee, M. A., Shapiro, V. D., and Sagdeev, R. Z. (1996). Pickup ion energization by shock surfing. *jgr*, 101:4777–4790.

Lindsay, B. G. and Stebbings, R. F. (2005). Charge transfer cross sections for energetic neutral atom data analysis. *Journal of Geophysical Research (Space Physics)*, 110:A12213.

McComas, D., Ebert, R., Elliott, H., Goldstein, B., Gosling, J., Schwadron, N., and Skoug, R. (2008). Weaker solar wind from the polar coronal holes and the whole sun. *Geophysical Research Letters*, 35(18).

McComas, D., Elliott, H., Schwadron, N., Gosling, J., Skoug, R., and Goldstein, B. (2003). The three-dimensional solar wind around solar maximum. *Geophysical research letters*, 30(10).

McComas, D. J., Alexashov, D., Bzowski, M., Fahr, H., Heerikhuisen, J., Izmodenov, V., Lee, M. A., Möbius, E., Pogorelov, N., Schwadron, N. A., and Zank, G. P. (2012). The Heliosphere's Interstellar Interaction: No Bow Shock. *Science*, 336:1291.

McComas, D. J., Bzowski, M., Fuselier, S. A., Frisch, P. C., Galli, A., Izmodenov, V. V., Katushkina, O. A., Kubiak, M. A., Lee, M. A., Leonard, T. W., Möbius, E., Park, J., Schwadron, N. A., Sokół, J. M., Swaczyna, P., Wood, B. E., and Wurz, P. (2015). Local Interstellar Medium: Six Years of Direct Sampling by IBEX. *apjs*, 220:22.

Opher, M. (2015). Magnetized Jets Driven By the Sun: The Structure of the Heliosphere Revisited. In *APS Meeting Abstracts*, page YI3.004.

Parker, E. N. (1958). Dynamics of the interplanetary gas and magnetic fields. *The Astrophysical Journal*, 128:664.

Parker, E. N. (1960a). The Hydrodynamic Theory of Solar Corpuscular Radiation and Stellar Winds. *The Astrophysical Journal*, 132:821.

Parker, E. N. (1960b). The Hydrodynamic Treatment of the Expanding Solar Corona. *The Astrophysical Journal*, 132:175.

Parker, E. N. (1961). The stellar-wind regions. *The Astrophysical Journal*, 134:20.

Parker, E. N. (1963). Interplanetary dynamical processes. *New York, Interscience Publishers, 1963.*

Pauls, H. L. and Zank, G. P. (1997). Interaction of a nonuniform solar wind with the local interstellar medium 2. A two-fluid model. *Journal of Geophysical Research*, 102:19779–19788.

Pogorelov, N. V., Borovikov, S. N., Florinski, V., Heerikhuisen, J., Kryukov, I. A., and Zank, G. P. (2009). Multi-scale Fluid-Kinetic Simulation Suite: A Tool for Efficient Modeling of Space Plasma Flows. In Pogorelov, N. V., Audit, E., Colella, P., and Zank, G. P., editors, *Numerical Modeling of Space Plasma Flows: ASTRONUM-2008*, volume 406 of *Astronomical Society of the Pacific Conference Series*, page 149.

Pogorelov, N. V., Borovikov, S. N., Heerikhuisen, J., and Zhang, M. (2015). The Heliotail. *The Astrophysical Journal*, 812:L6.

Pogorelov, N. V., Funsten, H. O., McComas, D. J., Reisenfeld, D. B., and Schwadron, N. A. (2017). Structure of the Heliotail from Interstellar Boundary Explorer Observations: Implications for the 11-year Solar Cycle and Pickup Ions in the Heliosheath. *apj*, 836:238.

Ratkiewicz, R., Ben-Jaffel, L., and Grygorczuk, J. (2008). What Do We Know about the Orientation of the Local Interstellar Magnetic Field? In Pogorelov, N. V., Audit, E., and Zank, G. P., editors, *Numerical Modeling of Space Plasma Flows*, volume 385 of *Astronomical Society of the Pacific Conference Series*, page 189.

Richardson, J. D. (2008). Plasma temperature distributions in the heliosheath. *Geophysical Research Letters*, 35:L23104.

Richardson, J. D., Kasper, J. C., Wang, C., Belcher, J. W., and Lazarus, A. J. (2008). Cool heliosheath plasma and deceleration of the upstream solar wind at the termination shock. *National Journal*, 454:63–66.

Stone, E. (2008). Voyager 2 Observations of the Solar Wind Termination Shock and Heliosheath. In *37th COSPAR Scientific Assembly*, volume 37 of *COSPAR Meeting*, page 3046.

Stone, E. C., Cummings, A. C., McDonald, F. B., Heikkila, B. C., Lal, N., and Webber, W. R. (2005). Voyager 1 Explores the Termination Shock Region and the Heliosheath Beyond. *Science*, 309:2017–2020.

Stone, E. C., Cummings, A. C., McDonald, F. B., Heikkila, B. C., Lal, N., and Webber, W. R. (2013). Voyager 1 Observes Low-Energy Galactic Cosmic Rays in a Region Depleted of Heliospheric Ions. *Science*, 341:150–153.

Suess, S. T. and Nerney, S. (1991). Erratum:'Flow downstream of the heliospheric terminal shock, 1, irrotational flow" by Steven T. Suess and Steven Nerney [J. of Geophys. Res. 95, 6403-6412 (1990)]. 96:1883–1883.

Vasyliunas, V. M. and Siscoe, G. L. (1976). On the flux and the energy spectrum of interstellar ions in the solar system. *Journal of Geophysical Research*, 81:1247–1252.

Washimi, H., Zank, G. P., Hu, Q., and Tanaka, T. (2007). Three-dimensional MHD simulation of the dynamic heliosphere. In Shaikh, D. and Zank, G. P., editors, *Turbulence and Nonlinear Processes in Astrophysical Plasmas*, volume 932 of *American Institute of Physics Conference Series*, pages 153–158.

Webber, W. R. and McDonald, F. B. (2013). Recent Voyager 1 data indicate that on 25 August 2012 at a distance of 121.7 AU from the Sun, sudden and unprecedented intensity changes were observed in anomalous and galactic cosmic rays. *Geophysical Research Letters*, 40:1665–1668.

Witte, M. (2004). Kinetic parameters of interstellar neutral helium. Review of results obtained during one solar cycle with the Ulysses/GAS-instrument. *aap*, 426:835–844.

Zank, G., Heerikhuisen, J., Wood, B. E., Pogorelov, N., Zirnstein, E., and McComas, D. (2012). Heliospheric structure: The bow wave and the hydrogen wall. *The Astrophysical Journal*, 763(1):20.

Zank, G. P. (2015). Faltering Steps Into the Galaxy: The Boundary Regions of the Heliosphere. *Annual review of astronomy and astrophysics*, 53:449–500.

Zank, G. P., Heerikhuisen, J., Pogorelov, N. V., Burrows, R., and McComas, D. (2010). Microstructure of the Heliospheric Termination Shock: Implications for Energetic Neutral Atom Observations. *apj*, 708:1092–1106.

Zank, G. P., Hunana, P., Mostafavi, P., and Goldstein, M. L. (2014). Pickup Ion Mediated Plasmas. I. Basic Model and Linear Waves in the Solar Wind and Local Interstellar Medium. *The Astrophysical Journal*, 797:87.

Zank, G. P. and Pauls, H. L. (1996). Modelling the Heliosphere. *Space Science Reviews*, 78:95–106.

Zank, G. P., Pauls, H. L., Cairns, I. H., and Webb, G. M. (1996). Interstellar pickup ions and quasi-perpendicular shocks: Implications for the termination shock and interplanetary shocks. *Journal of Geophysical Research*, 101:457–478.

Zirnstein, E. and McComas, D. (2015). Using kappa functions to characterize outer heliosphere proton distributions in the presence of charge-exchange. *The Astrophysical Journal*, 815(1):31.

Zirnstein, E. J., Heerikhuisen, J., Funsten, H. O., Livadiotis, G., McComas, D. J., and Pogorelov, N. V. (2016). Local Interstellar Magnetic Field Determined from the Interstellar Boundary Explorer Ribbon. *The Astrophysical Journal*, 818:L18.

Zirnstein, E. J., Heerikhuisen, J., Zank, G. P., Pogorelov, N. V., McComas, D. J., and Desai, M. I. (2014). Charge-exchange Coupling between Pickup Ions across the Heliopause and its Effect on Energetic Neutral Hydrogen Flux. *The Astrophysical Journal*, 783:129.

Zirnstein, E. J. and McComas, D. J. (2015). Using Kappa Functions to Characterize Outer Heliosphere Proton Distributions in the Presence of Charge-exchange. *The Astrophysical Journal*, 815:31.